Simulation-based inference for pulsar-population synthesis

Michele Ronchi, Celsa Pardo Araujo, Vanessa Graber & Nanda Rea

ronchi@ice.csic.es
pardo@ice.csic.es
graber@ice.csic.es
rea@ice.csic.es

MAGNESIA
erc
European Research Council
Established by the European Commission
Institute of Space Sciences
CSIC IEEC
EXCELENCIA MARÍA DE MAEZTU
UAB
Universitat Autònoma de Barcelona

The neutron-star zoo

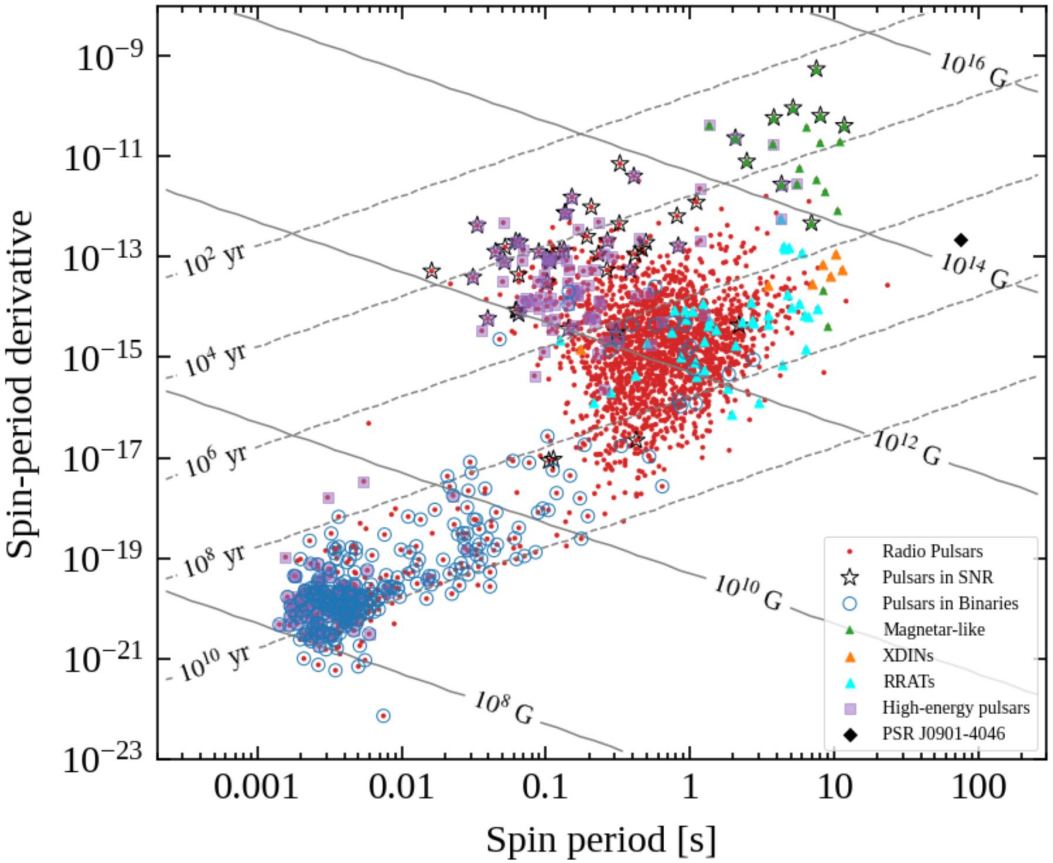

~ 3,000 pulsars are known to date

- Neutron stars are observed as pulsars across the electromagnetic spectrum from radio to X-rays and gamma-rays
- Different classes of neutron stars occupy different locations in the $P\dot{P}$-plane probing different evolution paths and/or different origins

data from the ATNF pulsar catalogue (Manchester et al. 2005)

ronchi@ice.csic.es

The neutron-star zoo

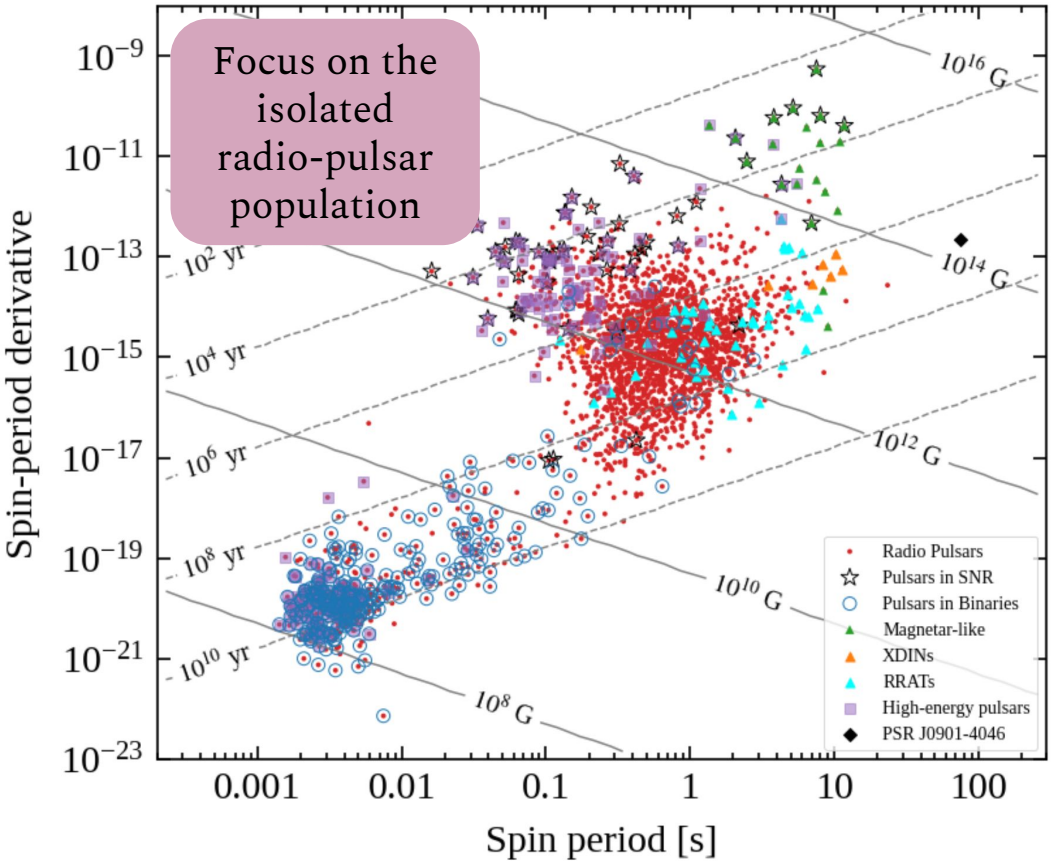

~ 3,000 pulsars are known to date

- Neutron stars are observed as pulsars across the electromagnetic spectrum from radio to X-rays and gamma-rays
- Different classes of neutron stars occupy different locations in the $P\dot{P}$-plane probing different evolution paths and/or different origins

data from the ATNF pulsar catalogue (Manchester et al. 2005)

ronchi@ice.csic.es

Population synthesis

CC supernova rate: ~ 2 per century × **Galaxy age:** ~ 13.6 billion years = **NS number:** ~ 2.8×10^8

(Rozwadowska et al. 2021)

- We only **detect** a very **small fraction** of all neutron stars.
  - What are the **natal properties** and the **birth rate** of the NS population?
  - Is there any **evolutionary link between different neutron-star classes**?

Population synthesis

CC supernova rate: ~ 2 per century (Rozwadowska et al. 2021) × **Galaxy age:** ~ 13.6 billion years = **NS number:** ~ 2.8×10^8

- We only **detect** a very **small fraction** of all neutron stars.
  - What are the **natal properties** and the **birth rate** of the NS population?
  - Is there any **evolutionary link between different neutron-star classes**?

- Population synthesis bridges this gap by focusing on the full population of neutron stars (e.g. Faucher-Giguère & Kaspi 2006, Lorimer et al. 2006, Gullón et al. 2014, Cieślar et al. 2020):

model **birth properties** with Monte-Carlo approach → **evolve properties** forward in time → **apply filters** to mimic observational biases/limits → **compare** mock simulations **to observations** to constrain input

Dynamical evolution

- **Neutron stars are born in star-forming regions**, i.e., in the Galactic disk along the Milky Way's spiral arms, **and receive kicks** during the supernova explosions.

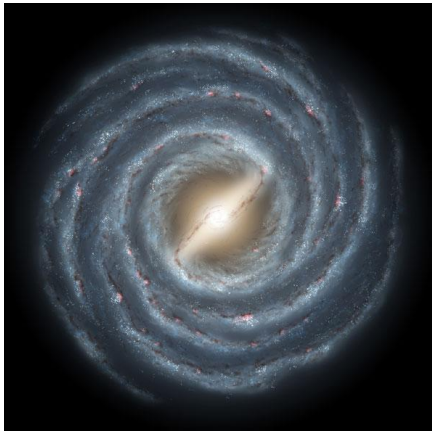

Artistic illustration of the Milky Way (credit: NASA JPL)

Dynamical evolution

- **Neutron stars are born in star-forming regions**, i.e., in the Galactic disk along the Milky Way's spiral arms, **and receive kicks** during the supernova explosions.

- We evolve the stars' position & velocity by **solving Newtonian equations of motion** in cylindrical galactocentric coordinates:

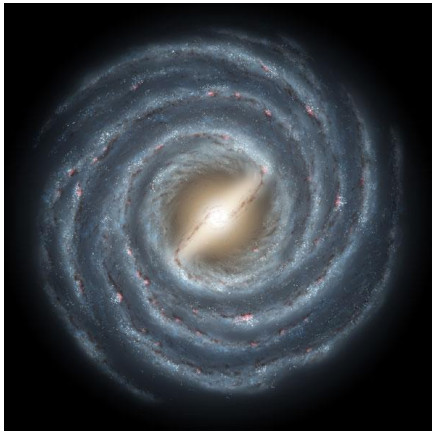

Artistic illustration of the Milky Way (credit: NASA JPL)

$$\ddot{\vec{r}} = -\vec{\nabla}\Phi_{\rm MW}$$

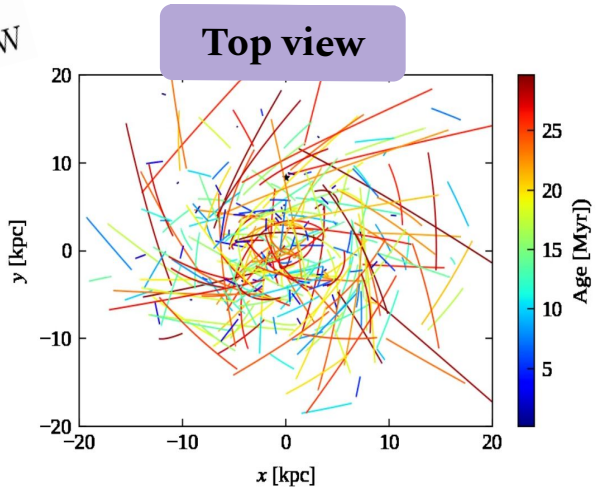

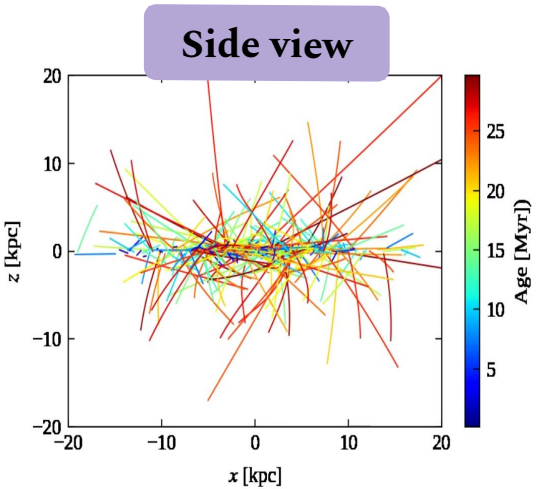

Magneto-rotational evolution

- The neutron-star magnetosphere exerts a **torque onto the star**. This causes **spin-down** and **alignment of the magnetic and rotation axes** (Spitkovsky 2006, Philippov et al. 2014).

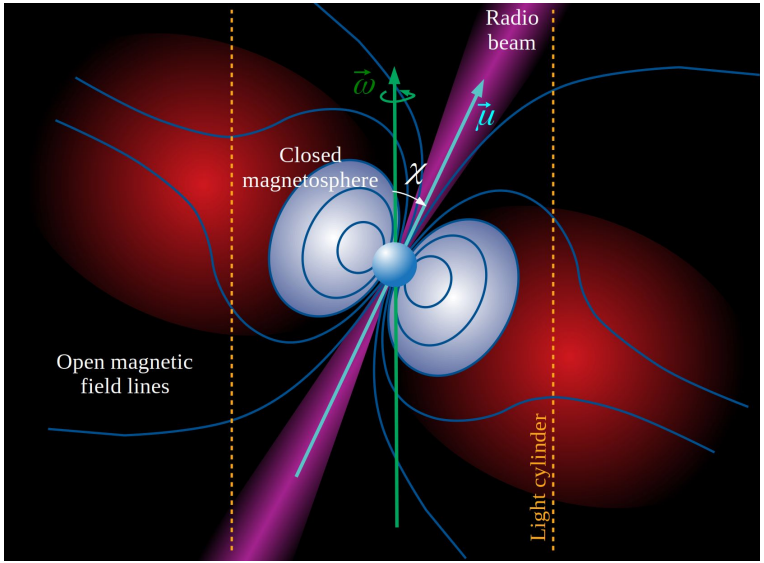

Magneto-rotational evolution

- The neutron-star magnetosphere exerts a **torque onto the star**. This causes **spin-down** and **alignment of the magnetic and rotation axes** (Spitkovsky 2006, Philippov et al. 2014).

- Neutron star **magnetic fields decay** due to the Hall effect and Ohmic dissipation in the outer stellar layer (crust) (e.g., Viganó et al. 2013 & 2021, De Grandis et al. 2020).

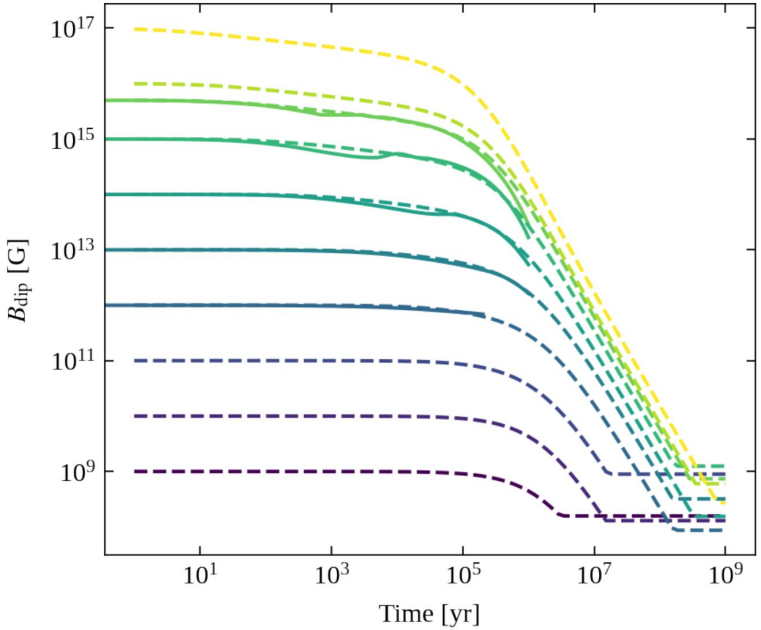

Magneto-rotational evolution

- The neutron-star magnetosphere exerts a **torque onto the star**. This causes **spin-down** and **alignment of the magnetic and rotation axes** (Spitkovsky 2006, Philippov et al. 2014).

- Neutron star **magnetic fields decay** due to the Hall effect and Ohmic dissipation in the outer stellar layer (crust) (e.g., Viganó et al. 2013 & 2021, De Grandis et al. 2020).

- We make the following assumptions:

  - **Initial periods** follow a normal in log with $\mu_{\log P}$ and $\sigma_{\log P}$ (Igoshev et al. 2022)
  - **Initial fields** follow a normal in log with $\mu_{\log B}$ and $\sigma_{\log B}$ (Gullón et al. 2014)
  - **Late-time decay of the B-field** follows a power-law with index α

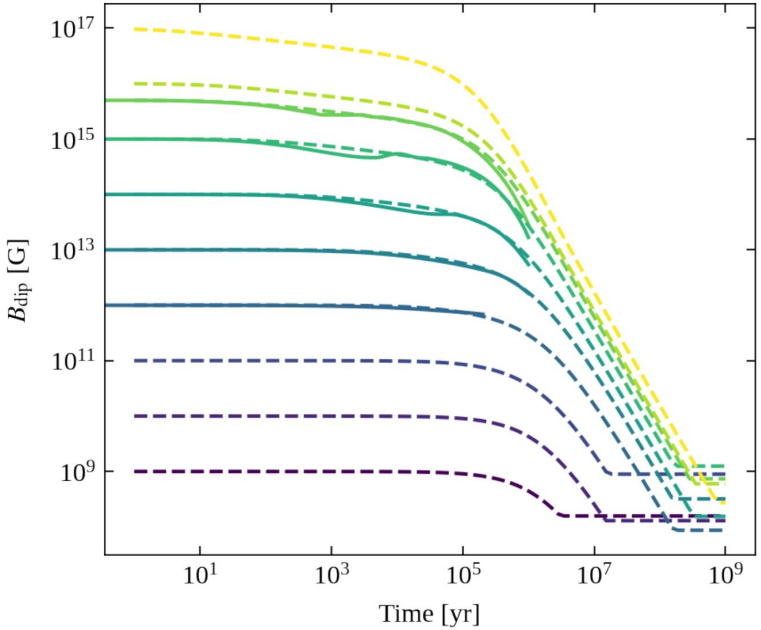

Magneto-rotational evolution

- The neutron-star magnetosphere exerts a **torque onto the star**. This causes **spin-down** and **alignment of the magnetic and rotation axes** (Spitkovsky 2006, Philippov et al. 2014).

- Neutron star **magnetic fields decay** due to the Hall effect and Ohmic dissipation in the outer stellar layer (crust) (e.g., Viganó et al. 2013 & 2021, De Grandis et al. 2020).

- We make the following assumptions:

  - **Initial periods** follow a normal in log with $\mu_{\log P}$ and $\sigma_{\log P}$ (Igoshev et al. 2022)
  - **Initial fields** follow a normal in log with $\mu_{\log B}$ and $\sigma_{\log B}$ (Gullón et al. 2014)
  - **Late-time decay of the B-field** follows a power-law with index α

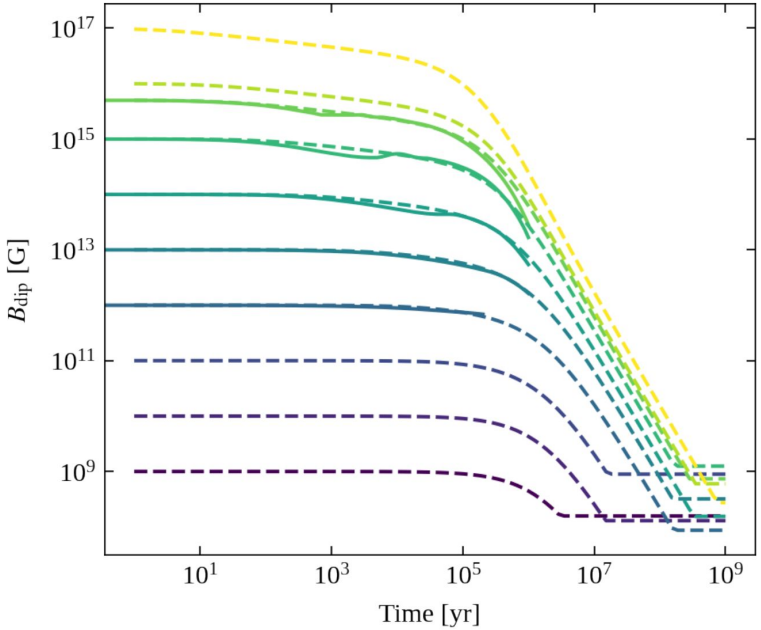

Here, we **vary** the five uncertain parameters $\mu_{\log P}$, $\sigma_{\log P}$, $\mu_{\log B}$, $\sigma_{\log B}$ and α.

Magneto-rotational evolution

$$\dot{P} = \frac{\pi^2}{c^3}\frac{B^2 R^6}{IP}\left(\kappa_0 + \kappa_1 \sin^2\chi\right)$$

$$\dot{\chi} = -\frac{\pi^2}{c^3}\frac{B^2 R^6}{IP^2}\left(\kappa_2 \sin\chi\cos\chi\right)$$

(Spitkovsky 2006,
Philippov et al. 2014)

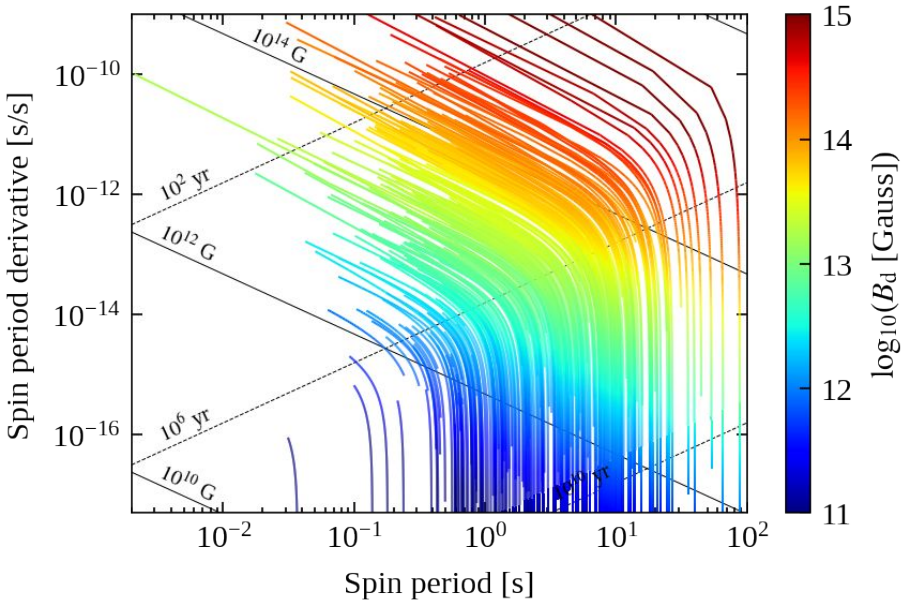

$P\dot{P}$ evolution tracks for
$\mu_{\log P}$ = -0.6 , $\sigma_{\log P}$ = 0.3 , $\mu_{\log B}$ = 13.25, $\sigma_{\log B}$ = 0.75 and α = *-2.0*

Radio emission and detection

- The stars' **rotational energy E_{rot}** is converted into coherent radio emission (Faucher-Giguère & Kaspi 2006; Gullón et al. 2014).

$$L_{\text{radio}} = L_0 \left(\frac{\dot{P}}{P^3} \right)^{1/2} \propto \dot{E}_{\text{rot}}^{1/2}$$

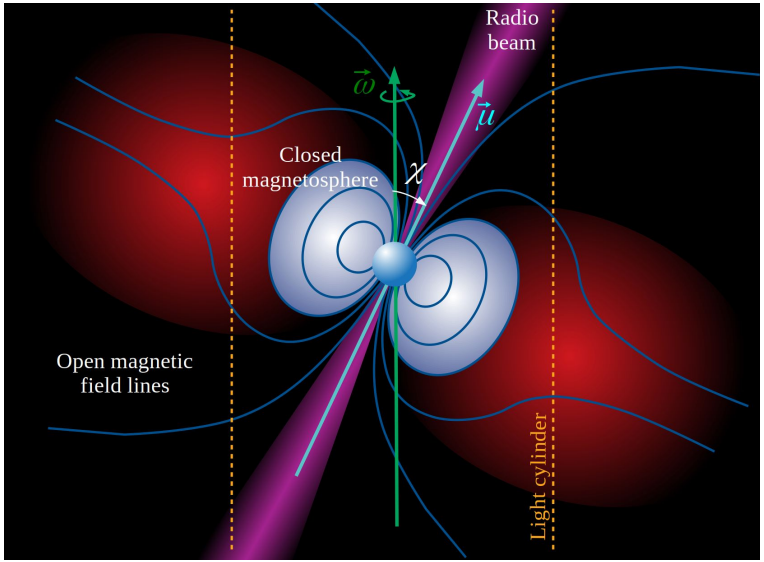

Radio emission and detection

- The stars' **rotational energy E_{rot}** is converted into coherent radio emission (Faucher-Giguère & Kaspi 2006; Gullón et al. 2014).

$$L_{\rm radio} = L_0 \left(\frac{\dot{P}}{P^3} \right)^{1/2} \propto \dot{E}_{\rm rot}^{1/2}$$

- As **emission is beamed**, ~ 90% of pulsars do not point towards us. For those intercepting our line of sight, compute **radio flux S_{radio}** & **pulse width W**.

$$S_{\rm radio} = \frac{L_{\rm radio}}{\Omega_{\rm beam} d^2}$$

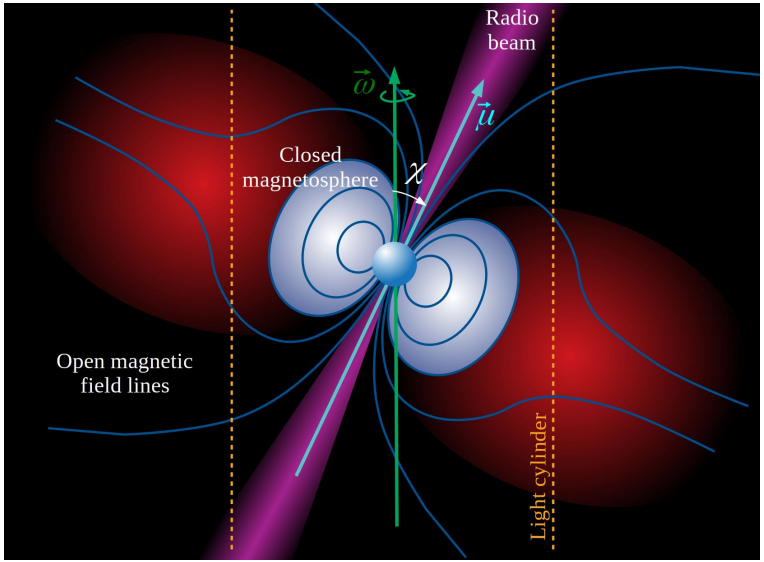

Radio emission and detection

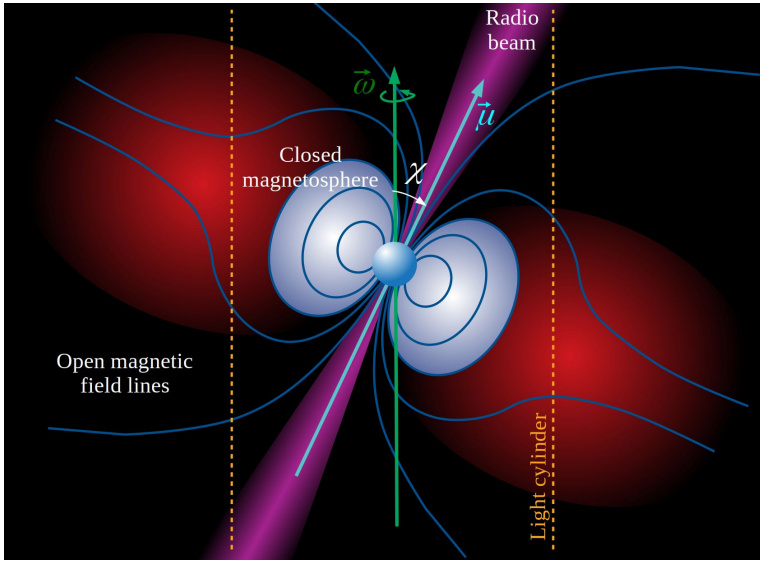

- The stars' **rotational energy E_{rot}** is converted into coherent radio emission (Faucher-Giguère & Kaspi 2006; Gullón et al. 2014).

$$L_{\rm radio} = L_0 \left(\frac{\dot{P}}{P^3} \right)^{1/2} \propto \dot{E}_{\rm rot}^{1/2}$$

- As **emission is beamed**, ~ 90% of pulsars do not point towards us. For those intercepting our line of sight, compute **radio flux S_{radio}** & **pulse width W**.

$$S_{\rm radio} = \frac{L_{\rm radio}}{\Omega_{\rm beam} d^2}$$

- A **signal-to-noise ratio** can be estimated through the **radiometer equation**.

$$S/N = \frac{S_{\rm mean} G \sqrt{N_{\rm pol} \Delta\nu \Delta t_{\rm obs}}}{\beta \left(T_{\rm rec} + T_{\rm sky}(l,b) \right)} \sqrt{\frac{P - w_{\rm eff}}{w_{\rm eff}}}$$

Radio emission and detection

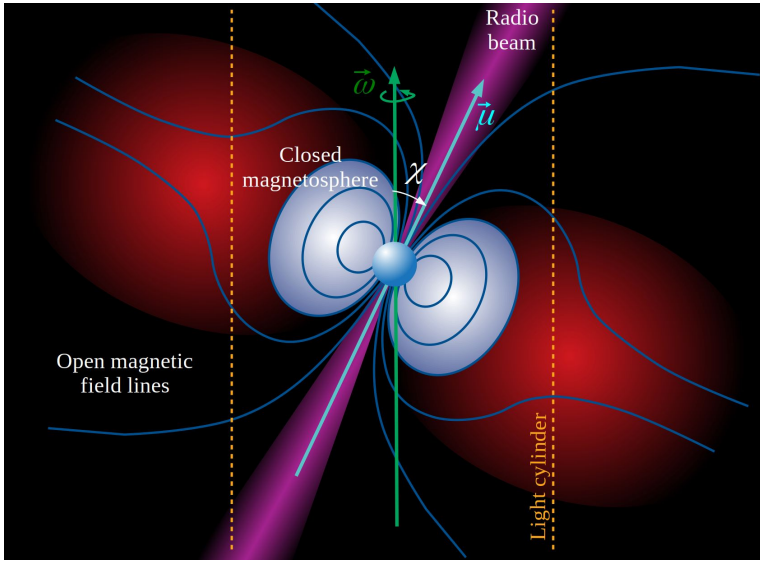

- The stars' **rotational energy E_{rot}** is converted into coherent radio emission (Faucher-Giguère & Kaspi 2006; Gullón et al. 2014).

$$L_{\rm radio} = L_0 \left(\frac{\dot{P}}{P^3} \right)^{1/2} \propto \dot{E}_{\rm rot}^{1/2}$$

- As **emission is beamed**, ~ 90% of pulsars do not point towards us. For those intercepting our line of sight, compute **radio flux S_{radio}** & **pulse width W**.

$$S_{\rm radio} = \frac{L_{\rm radio}}{\Omega_{\rm beam} d^2}$$

- A **signal-to-noise ratio** can be estimated through the **radiometer equation**.

$$S/N = \frac{S_{\rm mean} G \sqrt{N_{\rm pol} \Delta\nu \Delta t_{\rm obs}}}{\beta \left(T_{\rm rec} + T_{\rm sky}(l,b) \right)} \sqrt{\frac{P - w_{\rm eff}}{w_{\rm eff}}}$$

A pulsar counts as detected, if it **exceeds the sensitivity threshold** for a survey recorded with a specific radio telescope.

Three radio surveys

- We compare our simulated populations with three surveys from Murriyang (the Parkes Radio Telescope):
  - **Parkes Multibeam Pulsar Survey** (PMPS) (Manchester et al. 2001, Lorimer et al. 2006): *1,009 isolated pulsars*
  - **Swinburne Parkes Multibeam Pulsar Survey** (SMPS) (Edwards et al. 2001, Jacoby et al. 2009): *218 isolated pulsars*
  - **High Time Resolution Universe Survey** (HTRU) (Keith et al. 2018): *1,023 isolated pulsars*

Can we constrain birth properties by looking at a current snapshot of the pulsar population?

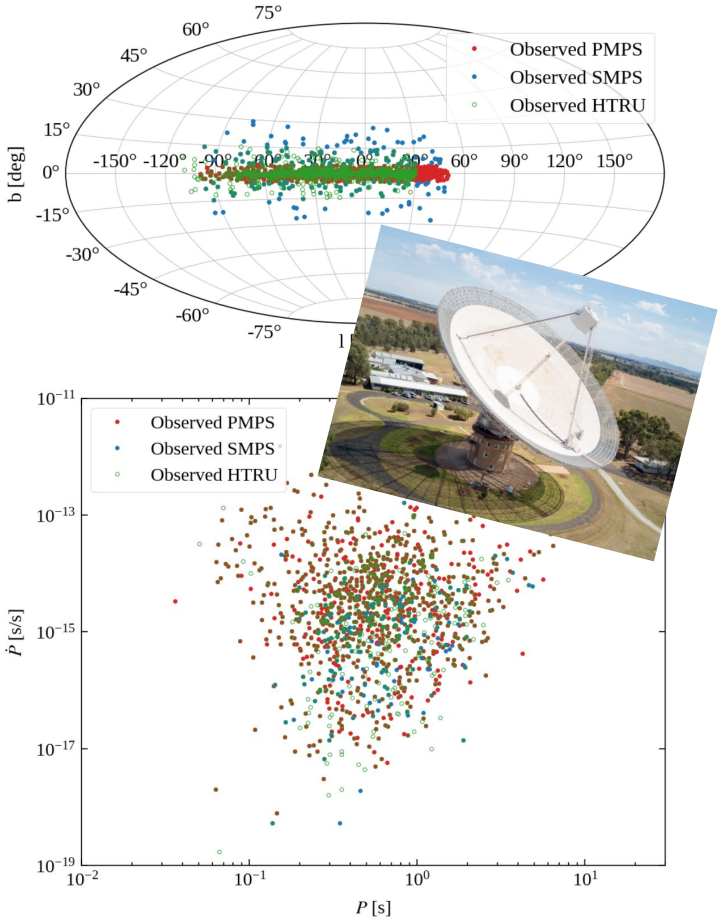

Simulation-based (likelihood-free) inference (SBI)

- Based on some prior knowledge $\pi(\theta)$, a stochastic model and some observation x, we want to infer the most likely distribution $P(\theta|x)$ for our model parameters θ given the data x. This is **encoded in Bayes' Theorem**:

$$\underbrace{\mathcal{P}(\theta|x)}_{\text{posterior}} = \frac{\overbrace{\mathcal{P}(\theta)}^{\text{prior } \pi} \overbrace{\mathcal{P}(x|\theta)}^{\text{likelihood } \mathcal{L}}}{\underbrace{\mathcal{P}(x)}_{\text{evidence}}}$$

For complex simulators, the **likelihood is defined implicitly and often intractable**. This is overcome with **simulation-based** (likelihood-free) **inference** (see e.g. Cranmer et al. 2020).

- Neural Posterior Estimation (NPE) (e.g., Papamakarios & Murray 2016) uses a neural network to learn a mapping between the simulated data and the posterior distribution of the underlying parameters.

SBI - Workflow

1. **sample** θ_i from the prior $\pi(\theta)$, for $i = 1, ..., N$

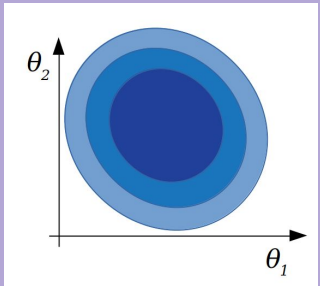

$(\mu_{\log P}, \sigma_{\log P}, \mu_{\log B}, \sigma_{\log B}, \alpha)$

SBI - Workflow

1. **sample** θ_i from the prior $\pi(\theta)$, for $i = 1, ..., N$

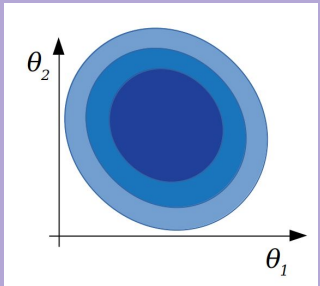

2. **run simulator** for θ_i to produce mock observations: $x_i \sim P(x|\theta_i)$

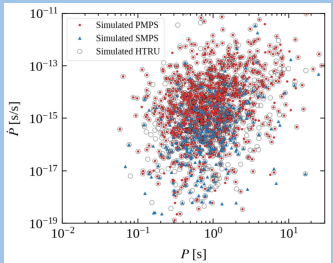

SBI - Workflow

1. **sample** θ_i from the prior $\pi(\theta)$, for $i = 1, ..., N$

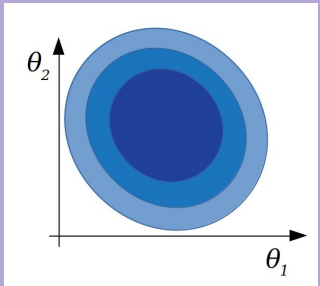

2. **run simulator** for θ_i to produce mock observations: $x_i \sim P(x|\theta_i)$

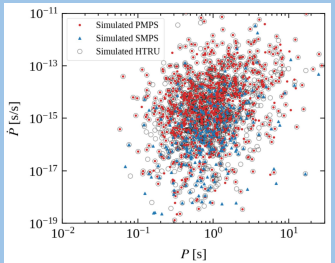

3. generate **summary statistics**: density maps of the three surveys in the $P\dot{P}$-plane

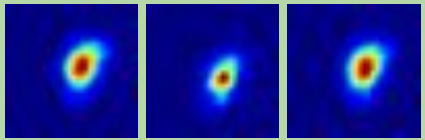

SBI - Workflow

1. **sample** θ_i from the prior $\pi(\theta)$, for $i = 1, ..., N$

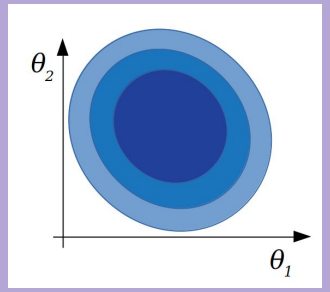

2. **run simulator** for θ_i to produce mock observations: $x_i \sim P(x|\theta_i)$

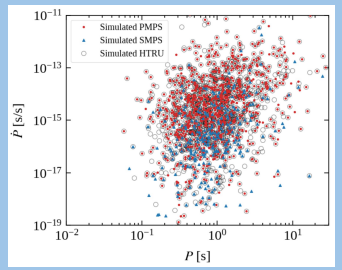

3. generate **summary statistics**: density maps of the three surveys in the $P\dot{P}$-plane

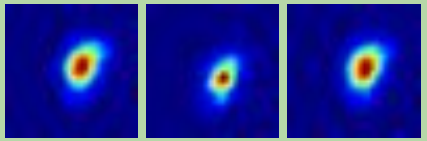

4. **train a neural network** (**conditional density estimator**) on simulated data to approximate the posterior

Tejero-Cantero et al. 2020

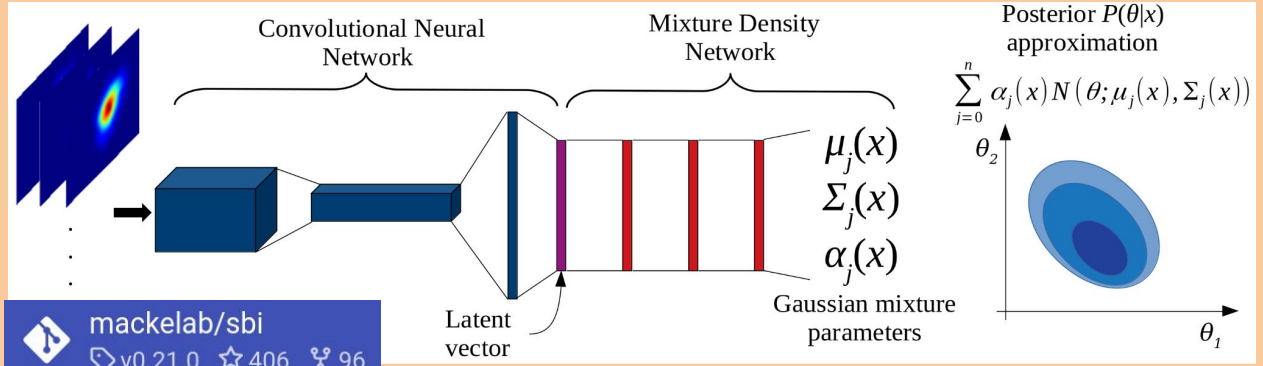

SBI - Results

- 120,000 simulations in total, we use 87 % for training, 10 % for validation, 3 % for testing.

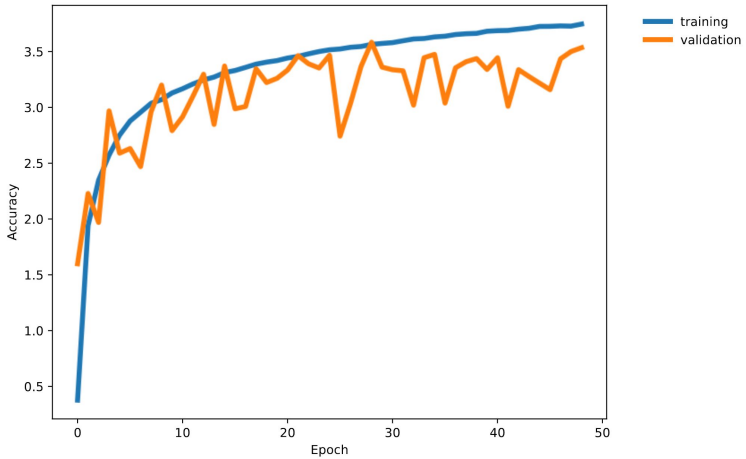

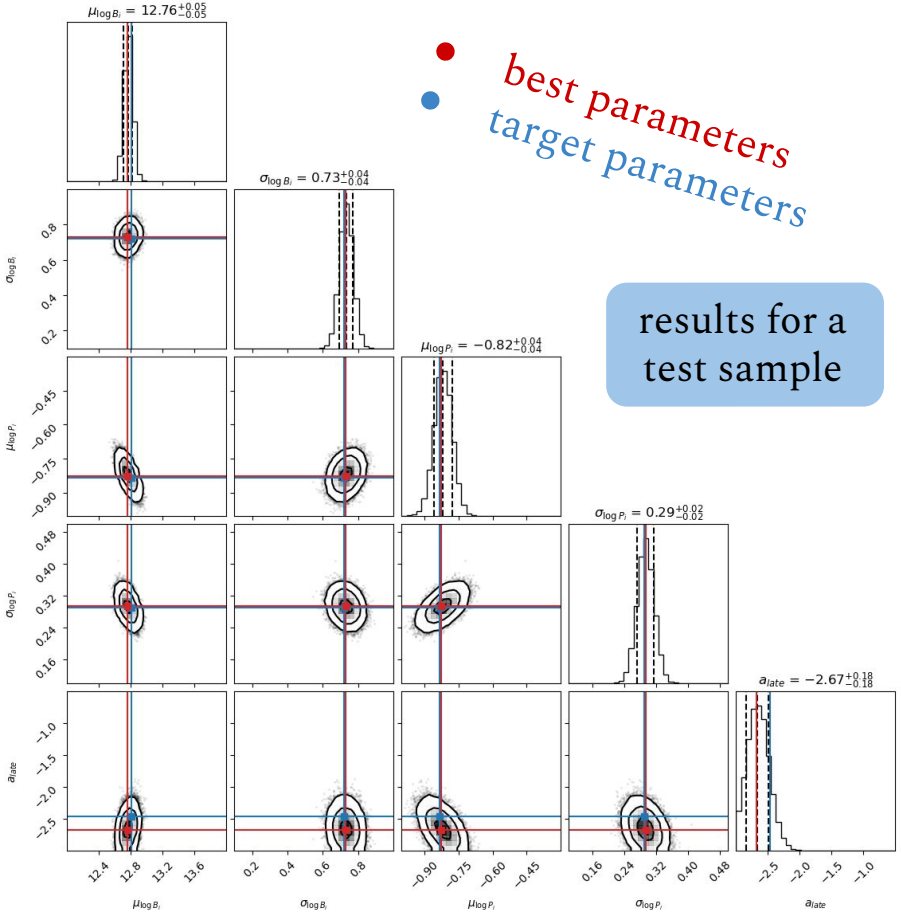

The network is able to predict the posterior for any input simulation (amortized posterior).

SBI - Results for observed population

With our optimised neural network, we can also **infer the posteriors** for the **pulsar population detected in our three surveys** and recover the following constraints:

$$\mu_{\log B} = 13.10^{+0.06}_{-0.06}$$
$$\sigma_{\log B} = 0.43^{+0.03}_{-0.03}$$
$$\mu_{\log P} = -0.93^{+0.12}_{-0.12}$$
$$\sigma_{\log P} = 0.40^{+0.14}_{-0.14}$$
$$\alpha = -1.92^{+0.25}_{-0.25}$$

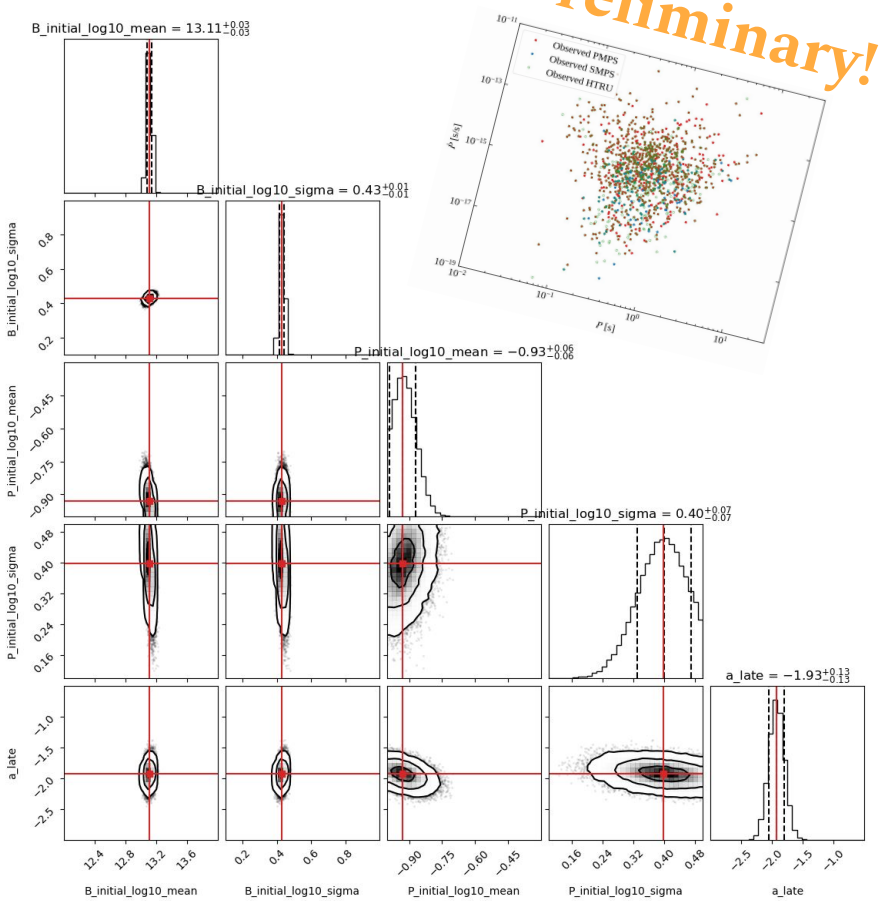

Future plans

IMPROVING THE SIMULATOR

- Explore **different assumptions on initial** period and magnetic-field **distributions**
- Extend framework to model also gamma-ray and X-ray emission and **predict the multi-wavelength emission**

IMPROVING SBI

- Expand the approach to **active learning** and derive posteriors sequentially **using SNPE.**

Thank you!

ronchi@ice.csic.es
pardo@ice.csic.es
graber@ice.csic.es
rea@ice.csic.es